HHS Public Access

Author manuscript

Plast Reconstr Surg. Author manuscript; available in PMC 2018 April 01.

Published in final edited form as:

Plast Reconstr Surg. 2017 April ; 139(4): 900e–910e. doi:10.1097/PRS.0000000000003187.

Human Adipose-Derived Stem Cells Labeled with Plasmonic Gold Nanostars for Cellular Tracking and Photothermal Cancer Cell Ablation

Ronnie L. Shammas, BS[*], **Andrew M. Fales, BS**[*], **Bridget M. Crawford, BS**, **Amy J. Wisdom, BS**, **Gayathri R. Devi, Ph.D.**, **David A. Brown, M.D, Ph.D.**, **Tuan Vo-Dinh, Ph.D**[Ψ], and **Scott T. Hollenbeck, M.D.**[Ψ]

Abstract

Background—Nanoparticles show promise within the field of cancer therapeutics. Among the nanoparticle constructs, gold nanostars (GNSs) are unique nanoplatforms that can be imaged in real-time and transform light energy into heat to ablate cells. However, targeted delivery of GNSs to tumors remains a challenge. Adipose-derived stem cells (ASCs) migrate towards tumor niches in response to chemokines. The ability of ASCs to migrate and integrate into tumors makes them ideal vehicles for the targeted delivery of cancer nanotherapeutics.

Methods—To test the labeling efficiency of GNSs, undifferentiated ASCs were incubated with GNSs and a commercially available nanoparticle (Qtracker), then imaged using two-photon photoluminescence (TPL) microscopy. The effects of GNSs on cell phenotype, proliferation, and viability was assessed with flow cytometry, MTT metabolic assay, and trypan blue respectively. Tri-lineage differentiation of GNS-ASCs was induced with the appropriate media. For cellular ablation, photothermolysis was performed on ASCs cultured alone or in co-culture with SKBR3 cancer cells.

Results—Efficient uptake of GNSs occurred in ASCs, with persistence of the luminescent signal over 4-days. Labeling efficiency and signal quality was greater than Qtracker. GNSs did not affect cell phenotype, viability, or proliferation, and exhibited stronger luminescence than Qtracker throughout differentiation. Zones of complete ablation surrounding the GNS-ASCs were observed following photothermolysis in both monoculture and co-culture models.

Conclusions—These studies show that GNSs effectively label ASCs without altering cell phenotype. Once labeled, photoactivation of GNS-ASCs ablates neighboring cancer cells, demonstrating the potential of ASCs as a vehicle for the delivery of site-specific cancer therapy.

Introduction

The relationship between adipose tissue and cancer is an area of active investigation. Perivascular progenitor cells, termed adipose-derived stem cells (ASCs), are recognized as key contributors to tumor progression. ASCs exhibit directional migration in response to chemokines released from the tumor microenvironment[1-6]. While the underlying biological

[Ψ]Corresponding authors: tuan.vodinh@duke.edu and scott.hollenbeck@duke.edu.
[*]These authors contributed equally to this work

mechanisms of tumor-specific ASC migration are largely unknown, studies have suggested various contributory pathways such as SDF-1/CXCR4, PDGF-BB/PDGFR- β, CCR5/RANTES, IGF1R/IGF, and IL8R/IL-8 [7-10]. Further clarification of these pathways has led to increasing interest in the use of tumor-localizing ASCs for site-specific gene therapy and nanoparticle and drug delivery [11-13]. Growing evidence also suggests that ASCs facilitate tumor growth, angiogenesis, immune evasion, and metastasis[2, 14, 15]. Inflammatory chemokines found in the tumor microenvironment may be responsible for the integration of ASCs into the tumor stroma [16]. It is thought that the tumor microenvironment may simulate a site of chronic inflammation, resulting in the increased secretion of soluble factors that are responsible for promoting the integration of ASCs into the tumor stroma[16, 17]. This concept has been demonstrated in *in vitro* mammosphere models, and partially elucidated in *in vivo* models as well [17, 18]. The unique ability of ASCs to migrate and integrate into tumors makes them ideal vehicles for the targeted delivery of cancer therapeutics.

The development of a targeted delivery system that effectively utilizes ASCs requires both the ability to track ASCs from the point of entry through migration to the tumor and a therapeutic strategy that exploits the ability of ASCs to localize to the tumor cells. Our group has investigated the use of a novel nanoparticle for tracking ASCs while exploiting this optical label in a unique therapeutic approach.

With respect to cell tracking, one obstacle limiting the use of ASCs is the inability to monitor live cells in real-time at multiple time points [19, 20]. The current gold standard cellular label, Qtracker (red-fluorescent Qdot® 655 nanocrystals, Invitrogen, Waltham, MA), permits short-term cell tracking but does not provide high spatial resolution, limiting its use for whole-body imaging[21]. A nanoparticle with a more sensitive imaging capability would allow for in-situ localization of cells within a given tumor. This would allow for the use of stem cells, or other cells, to be efficiently monitored when used as a cancer therapeutic in experimental or clinical trials.

Our laboratory has developed unique plasmonic-active nanoplatforms known as gold nanostars (GNSs) that are synthesized without cytotoxic chemicals (such as free cetyltrimethylammonium bromide), and accumulate intracellularly via micropinocytosis following conjugation with the transactivator of transcription (TAT) peptide[22-24]. In addition, the unique two-photon luminescence (TPL) of GNSs allows for direct particle visualization under multiphoton microscopy, as well as real-time imaging[23].

In addition to the TPL properties, the GNSs are able to efficiently transform non-harmful light energy into heat to thermally ablate cells[22, 25]. The concept of photothermal ablation involves the application of a low-intensity laser (to the surface of the skin) to activate nanoparticles localized within deeper tissues. These nanoparticles subsequently convert the light energy into heat, triggering thermal ablation with ensuing cell death[22, 26].

Efficient photothermal ablation requires an even GNS distribution within the target tissue[27]. The recently described tumor-targeting effect of stem cells suggests their use as

site-specific drug carriers to deliver GNSs to the tumor site, resulting in an even intratumoral nanoparticle distribution[28].

The research reported here includes the following: (1) determination of whether GNSs alter the stem-like phenotype of ASCs; (2) investigation of the use of GNSs as long-term TPL labels to monitor ASCs throughout tri-lineage differentiation; and (3) demonstration of the feasibility of using GNS-labeled ASCs (GNS-ASCs) as targeted platforms for efficient photothermal ablation of stem cells and surrounding cancer cells in a co-culture model.

Materials and Methods

Cell Lines and Culture Conditions

Human ASCs were purchased from Zen-Bio (Zen-Bio Inc.; Research Triangle Park, NC, USA) and maintained in pre-adipocyte medium (PM-1; Zen-Bio Inc.). The ASCs were confirmed by the supplier using flow cytometry prior to shipment to stain >99% positive for CD105 and CD44; and negative for CD31 and CD45. SKBR3 cells (human adenocarcinoma of the breast, pleural effusion) were obtained from ATCC©. Cell lines were maintained at 37°C in 5% CO_2, and supplemented with fresh media (PM-1; Zen-Bio Inc.) every 2-3 days. ASCs from serial passages 2-5 were used for all experiments.

Gold Nanostar Preparation

All chemicals were purchased from Sigma-Aldrich (St. Louis, MO). GNSs were prepared by a surfactant-free method as described previously [22]. Briefly, citrate-capped gold seeds were prepared by adding 15mL of 1% trisodium citrate to 100mL of boiling $HAuCl_4$ solution (1mM) under vigorous stirring for 15 minutes. The solution was cooled to room temperature and filtered by a 0.22μm nitrocellulose membrane and stored at 4°C. GNSs were prepared by simultaneously mixing 1mL of 3mM $AgNO_3$ and 500μL of 0.1M ascorbic acid into 100mL of 0.25mM $HAuCl_4$ containing HCl (100μL, 1N) and citrate gold seeds (1mL, OD_{520}: 2.8). PEG-GNSs was prepared by adding 5μM of $SHPEG_{5000}$ (*O*-[2-(3mercaptopropionylamino) ethyl]-*O′*-methylpolyethleneglycol) to freshly synthesized GNS for 15 minutes. Lastly, TAT-GNS were prepared by mixing a final solution of 100μM of cysteine-TAT-peptide (residues 49-57, sequence Arg-Lys-Lys-Arg-Arg-Arg-Gln-Arg-Cys-$CONH_2$, SynBioSci, Livermore, CA) with 1nM of PEG-GNS solution for 48 hours at 4°C followed by two centrifugal washes in ethanol.

Nanoparticle Uptake into Adipose-Derived Stem Cells

Solutions of GNSs and a commercially available nanoparticle cell label, Qtracker 625 (Invitrogen) were prepared for cellular incubation by suspending in PBS. Cells were incubated with the appropriate particle-containing solution (final concentration of 0.14nM) for 24 hours before experimental use.

Co-Culture of GNS-Labeled ASCs and SKBR3 Breast Cancer Cells

GNS-ASCs and SKBR3 cells were seeded at a ratio of 1:1 (20,000 cells/cm^2), incubated overnight, and supplemented with fresh PM-1 media prior to laser treatment.

Flow Cytometry

The surface antigens of unlabeled ASCs, as compared to GNS-labeled ASCs, were characterized by flow cytometry. 1×10^6 cells/tube were stained with monoclonal antibodies against CD90 (APC), CD105 (PE), CD45 (PE-Cy5) and IgG1 control, CD31 (AF-700) and IgG1 control, and CD44 (BV-421). All antibodies were purchased from BioLegend, San Diego, CA. Analysis was performed on a BD LSRII cytometer (Becton Dickinson, San Jose, CA). For each sample, 100,000 events were collected; the data was analyzed with FlowJo (TreeStar).

Two-Photon Photoluminescence Comparison between GNS-labeled ASCs and Qtracker-Labeled ASCs

Following labeling of ASCs with GNS and Qtracker, cells were plated and supplemented daily with fresh growth media. On the 1st, 2nd, and 4th days, the plates were fixed with 4% paraformaldehyde before imaging by multiphoton microscopy (MPM). To assess intracellular particle distribution, the cells were stained with Hoechst33342 (Invitrogen). The degree of calculated total cell TPL was derived using ImageJ as previously performed [29].

Multilineage Differentiation of GNS-labeled ASCs

GNS-labeled ASCs were analyzed for their capacity to differentiate along adipogenic, osteogenic, and chondrogenic lineages and monitored using MPM. In all samples, the TPL signal of GNS was compared to Qtracker over 21 days. For both adipogenesis and osteogenesis, the cells were maintained in PM-1 media until approximately 100% confluent. The cells were then differentiated using adipocyte (DM-2, Zen-Bio Inc.) and osteoblast (OB-1, Zen-Bio Inc.) differentiation media. Complete adipogenic and osteogenic differentiation was evaluated using Oil Red O and Alizarin red S staining, respectively. For chondrogenesis, a micromass culture protocol was used. A 25μL droplet (80,000 cells) was placed in the center of each well, incubated for 2 hours at 37°C, and then supplemented with 2mL of chondrocyte differentiation media (CM-1, Zen-Bio Inc.) for 21 days. Alcian blue stain was used to confirm differentiation. On the 7th and 21st days of differentiation, images were taken with the MPM to monitor the TPL emitted from GNS and Qtracker.

Multiphoton Microscopy Imaging

All MPM images were taken using a multiphoton microscope (Olympus FV1000, Olympus America, Center Valley, PA) at the Light Microscopy Core Facility, Duke University. Imaging was carried out with a femtosecond Ti:Sapphire laser (Chameleon Vision II, Coherent, Santa Clara, CA) with tunable range 680-1080nm, a 140fsec pulse width and 80MHz repetition rate. Images were taken under 800nM excitation and 3.7mW unless otherwise noted. All images were collected and reconstructed using ImageJ[30].

Trypan Blue Cell Viability and MTT Proliferation Assays

A trypan blue viability assay was used to distinguish the number of live and dead cells in undifferentiated ASCs labeled with GNSs and Qtracker. Concentrations of 0.05nM, 0.1nM, and 0.14nM of GNSs and Qtracker were incubated with ASCs for 24 hours; dead cells were enumerated using the Cellometer® Auto 2000 (Nexcelom).

A MTT (Sigma) assay was used to compare cellular proliferation in undifferentiated ASCs labeled with GNSs and Qtracker. In this assay, MTT (3-(4, 5-dimethylthiazolyl-2)-2, 5-diphenyltetrazolium bromide) is reduced by metabolically active cells and quantified by spectrophotometry. Concentrations of 0.05nM, 0.1nM, and 0.14nM of GNSs and Qtracker were used. The absorbance was determined using a spectrophotometer (FLUOstar Optima, BMG Biotech).

In Vitro Photothermal Therapy

ASCs were incubated with GNSs and then seeded into 35mm Petri dishes. For photothermal therapy, cells on a 37°C heating stage of a MPM were exposed to the 800-nm wavelength of a Ti:Sapphire laser at output powers of 2.19mW, 3.7mW, or 9.14mW for 3 minutes. ASCs cultured with untreated media were used as controls and received the same laser treatment. Immediately after treatment, cells were examined under a fluorescence microscope using fluorescein diacetate and propidium iodide.

Photothermal therapy was applied to GNS-ASC and cancer cell co-cultures. For photothermal therapy, cells were kept on a 37 °C heating stage and exposed to an 800-nm laser at 3.7mW for 3 minutes. Cancer cells cultured with unlabeled ASCs were used as controls and received the same laser treatment. Immediately after treatment, cells were examined using fluorescein diacetate and propidium iodide.

Statistical Analysis

Data are expressed as means ± SEM. Statistical comparisons of the calculated degree of two-photo luminescence were analyzed with GraphPad Prism 6 (GraphPad Software, La Jolla, California, USA) using a two-way ANOVA. Furthermore, a student's *t* test was used for analysis of proliferation and viability data. A value of $p < 0.05$ was considered statistically significant.

Results

Signal Intensity is Higher for GNS-Labeled ASCs than for Qtracker-Labeled ASCs Throughout Proliferation

In vitro experiments were performed to assess the localization of GNSs into ASCs and to directly compare GNSs to Qtracker as an optical label. Figure 1 (*top*) demonstrates the predominant TPL signal of GNSs in the ASC cytoplasm, visualized using MPM. Figure 1 (*bottom*) displays the TPL signal profiles of both GNSs (white) and Qtracker (red) in ASCs over 4 days. Although TPL signals of both Qtracker and GNSs decreased overtime, the signal intensity was higher for the GNS-labeled ASCs. In addition, the rate of signal decay was decreased for cells labeled with GNSs. Statistical analysis using a two-way ANOVA showed a significantly higher degree ($P<0.0001$) of integrated total cell TPL signal throughout the 4-day period in GNS-labeled ASCs.

Effects of Intracellular GNS Accumulation on ASC Phenotype and Viability

Flow cytometry demonstrated that GNSs did not alter ASC surface antigens (see Figure, Supplemental Digital Content 1, *top* which displays results from flow cytometry, INSERT

LINK). GNS-ASCs maintained expression of CD44 (98.2%), CD90 (98.2%), and CD105 (99.1%) after labeling. In addition, GNS-ASCs were negative for hematopoietic cell markers CD45 (0.46%) and CD31 (0.40%), which confirms the mesenchymal stem cell origin. Trypan blue and MTT assays were conducted to determine the effect of GNSs on undifferentiated ASC viability and proliferation.

MTT assays demonstrated no significant difference in cellular proliferation between cells labeled by Qtracker and those labeled by GNSs (see Figure, Supplemental Digital Content 1, *bottom left* which displays the results from proliferation assays, INSERT LINK). Increasing concentrations of both optical labels had no significant effects on cellular proliferation. Trypan blue viability assays demonstrated that concentrations of both Qtracker and GNSs, up to and including 0.1nM, had no significant effects, but at a concentration of 0.14nM, viability had decreased slightly (see Figure, Supplemental Digital Content 1, *bottom right* which displays the results from the viability assay, INSERT LINK).

GNSs Are Visualized Throughout Tri-Lineage Differentiation of ASCs

To evaluate whether GNS-ASCs maintain the capacity for tri-lineage differentiation, GNS-ASCs were cultured in lineage-specific differentiation media for 21 days. Qtracker-labeled ASCs were also differentiated to compare the TPL properties of both optical labels (Figure 2). After 21 days, cells were stained to validate their differentiated phenotype. In addition, images were captured using MPM throughout differentiation. Imaging began at 7 days for adipogenesis (Figure 2), osteogenesis, and chondrogenesis. GNS-labeled cells exhibited strong TPL throughout differentiation, with only slight decay in signal over time. Therefore, the decrease in signal intensity in these GNS-labeled cells did not preclude the use of MPM. In comparison, Qtracker-labeled cells exhibited such rapid signal decay that by the 21st day, cells were not easily visualized (Figure 2). Analysis of GNS and Qtracker-labeled cells using a two-way ANOVA demonstrated significantly greater TPL ($p < 0.001$) for GNS throughout tri-lineage differentiation. Lastly, the cytoplasmic localization of the GNS remained undisrupted in all three lineages as demonstrated with Hoechst33342 staining.

GNS-ASCs are Photoactivated, Killing ASCs and Surrounding Cancer Cells

Live/dead fluorescent staining was used to determine whether the photothermal response generated by GNS-ASCs was robust enough to induce thermolysis after laser photoactivation at varying intensities. The unlabeled ASCs were fully viable after all treatments, while the GNS-ASCs demonstrated significant cell death (Figure 3). The most efficient treatment method was found to be 3 minutes with a laser power of 3.7mW. In co-culture experiments of GNS-ASCs with SKBR3 cells, a distinct area of ablation was seen. Dead cells (stained red) had a tendency to remain in the center of the zone of ablation or detach from the treated area (Figure 4). Co-cultures of unlabeled ASCs and SKBR3 cells demonstrated no cell death following photothermal treatment.

Discussion

This study demonstrates that GNSs can effectively label ASCs in both undifferentiated and differentiated states without significantly altering cell phenotype and viability. The data also

confirm that the high photothermal conversion efficiency of GNSs generates enough thermal energy to kill nanoparticle-containing stem cells and surrounding breast cancer cells.

The small size and sensitive imaging properties of gold nanoparticles have made them increasingly attractive for cellular imaging and cancer therapy[31, 32]. Because tumor cells are highly susceptible to heat, hyperthermic therapy as an adjunctive treatment for cancer has been previously investigated[33, 34]. Under laser exposure, the GNS absorbs light energy and converts it to heat, which disrupts the cell membrane and causes cell ablation [35]. However, success with nanoparticle-based therapeutics has been limited due to heterogeneous tumoral distribution of the nanoparticles. Stem cell mediated GNS delivery may provide a solution to this problem. It is well established that stem cells of mesenchymal origin demonstrate tropism to tumors[36-38]. This property has generated increased interest in the use of stem cells as vehicles for targeted drug delivery; however, one obstacle to the development of stem cell therapies is the inability to track administered cells *in vivo* over a prolonged period of time. The authors of this study aimed to investigate the use of GNSs as a vividly fluorescent stem cell label, and potential cancer therapeutic when delivered with ASCs.

Snapshot images of cell location are insufficient to fully elucidate the migration, differentiation, and proliferative fate of transplanted cells [39, 40]. To confirm the proper migration of stem cells to their target in clinical practice, reliable imaging techniques are required[41, 42]. This study indicates that GNSs provide a strong TPL signal over a clinically relevant time course, which can be employed to track labeled stem cells utilized in a therapeutic application. Prior studies have shown that GNSs can also be visualized *in vivo* using multiple modalities of whole-body imaging including PET, CT, and MRI [43]. The unique ability of this gold nanoparticle to be imaged for an extended period of time across multiple imaging platforms will provide the most comprehensive information for stem cell therapy in the clinical setting [20, 44-46].

The application of TPL microscopy as a noninvasive imaging technique of living tissues has garnered significant interest due to the high signal-to-noise ratio in nanoparticle imaging. Qtracker is one of the most promising commercially available TPL labels available for cellular tracking. However, there are several drawbacks to Qtracker that limit its *in vivo* use, including multi-exponential signal decay and relative cytotoxicity [47, 48]. Our studies demonstrate that GNSs exhibit a superior intracellular retention and stronger TPL signal in both differentiated and undifferentiated cells. Throughout proliferation and differentiation, the fluorescent properties of GNS-labeled cells were easily detected; while cells labeled with Qtracker displayed significant signal decay. The large size of the GNSs and resulting cellular retention may account for the higher longevity and degree of TPL signal intensity as compared to Qtracker[49, 50].

The gold nanostars used in these studies are advantageous because, in addition to their luminescent signal, these nanoparticles have a high photon-to-heat conversion efficiency that allows for their potential application in cancer therapy [44, 47]. This allows for superior nanotherapeutic capabilities in comparison to other commonly used nanoparticles [23, 51-54].

To successfully implement the use of stem cells as nanoparticle carriers, it is important to load cells with GNSs without significantly altering their intrinsic properties or reducing viability[28]. Our data demonstrate that GNSs do not alter the phenotype of ASCs and do not impede differentiation. Our studies suggest a slight decrease in cell viability following a 24-hour incubation with either GNSs or Qtracker, indicating that significant cell death may occur at higher concentrations.

The concept of using cells as a delivery mechanism has proven to be an effective method to achieve an even distribution of nanoparticles at the tumor site, which is essential for therapeutic photothermal ablation [27, 55-58]. However, there has been no previous investigation of ASC-assisted targeted delivery of GNSs for photothermal ablation. Previous studies have focused on the use of bone marrow derived mesenchymal stem cells and neural stem cells, neither of which is as readily accessible for clinical use as ASCs, which can be easily harvested from the subcutaneous fat of patients[59-61]. In addition, other studies have focused on the use of nanorods and nanoshells, both of which are less effective in photothermal treatment than GNSs[62]. As demonstrated in our studies, the nanoparticles in the ASCs produce enough heat to ablate not only the stem cells, but also surrounding cancer cells. The long term goal of this project is to provide therapeutic delivery GNS-ASCs, which then migrate to the tumor bed and can be noninvasively photoactivated to ablate cancer cells by laser pulsation through the overlying skin. The work presented in this study establishes the basis for future *in vivo* models investigating stem cell delivery of GNSs to tumor sites, with subsequent photothermal ablation of cancer.

Conclusions

GNS-ASCs exploit the tumor tropism of ASCs, which may allow for site-specific photothermal ablation in cancer therapy. This study demonstrates efficient uptake of GNSs by ASCs and TPL signal persistence over 21 days in culture, as well as minimal effects of the nanoparticle on cell viability, proliferation, and multilineage differentiation. Photothermal ablation was effective in destroying labeled ASCs and neighboring cancer cells, though it did not appear to harm unlabeled cells. Future studies will employ an *in vivo* breast cancer mouse model to optimize tracking and photothermal ablation of the GNS-ASCs following implantation.

Supplementary Material

Refer to Web version on PubMed Central for supplementary material.

References

1. Zuk PA. The adipose-derived stem cell: looking back and looking ahead. Molecular biology of the cell. 2010; 21:1783–1787. [PubMed: 20375149]
2. Freese KE, Kokai L, Edwards RP, et al. Adipose-derived stems cells and their role in human cancer development, growth, progression, and metastasis: a systematic review. Cancer research. 2015; 75:1161–1168. [PubMed: 25736688]
3. Jeon JY, An JH, Kim SU, Park HG, Lee MA. Migration of human neural stem cells toward an intracranial glioma. Exp Mol Med. 2008; 40:84–91. [PubMed: 18305401]

4. Spaeth E, Klopp A, Dembinski J, Andreeff M, Marini F. Inflammation and tumor microenvironments: defining the migratory itinerary of mesenchymal stem cells. Gene Ther. 2008; 15:730–738. [PubMed: 18401438]

5. Shi M, Li J, Liao L, et al. Regulation of CXCR4 expression in human mesenchymal stem cells by cytokine treatment: role in homing efficiency in NOD/SCID mice. Haematologica. 2007; 92:897–904. [PubMed: 17606439]

6. Levesque JP, Hendy J, Takamatsu Y, Simmons PJ, Bendall LJ. Disruption of the CXCR4/CXCL12 chemotactic interaction during hematopoietic stem cell mobilization induced by GCSF or cyclophosphamide. The Journal of clinical investigation. 2003; 111:187–196. [PubMed: 12531874]

7. Freese KE, Kokai L, Edwards RP, et al. Adipose-Derived Stems Cells and Their Role in Human Cancer Development, Growth, Progression, and Metastasis: A Systematic Review. Cancer research. 2015; 75:1161–1168. [PubMed: 25736688]

8. Gehmert S, Gehmert S, Prantl L, Vykoukal J, Alt E, Song YH. Breast cancer cells attract the migration of adipose tissue-derived stem cells via the PDGF-BB/PDGFR-β signaling pathway. Biochemical and Biophysical Research Communications. 2010; 398:601–605. [PubMed: 20603108]

9. Bago JR, Alieva M, Soler C, Rubio N, Blanco J. Endothelial differentiation of adipose tissue-derived mesenchymal stromal cells in glioma tumors: implications for cell-based therapy. Mol Ther. 2013; 21:1758–1766. [PubMed: 23760448]

10. Choi SA, Lee JY, Kwon SE, et al. Human Adipose Tissue-Derived Mesenchymal Stem Cells Target Brain Tumor-Initiating Cells. PLoS ONE. 2015; 10

11. Gao Z, Zhang L, Hu J, Sun Y. Mesenchymal stem cells: a potential targeted-delivery vehicle for anti-cancer drug, loaded nanoparticles. Nanomedicine. 2013; 9:174–184. [PubMed: 22772046]

12. Cavarretta IT, Altanerova V, Matuskova M, Kucerova L, Culig Z, Altaner C. Adipose Tissue-derived Mesenchymal Stem Cells Expressing Prodrug-converting Enzyme Inhibit Human Prostate Tumor Growth. Mol Ther. 2009; 18:223–231. [PubMed: 19844197]

13. Bao Q, Zhao Y, Niess H, et al. Mesenchymal Stem Cell-Based Tumor-Targeted Gene Therapy in Gastrointestinal Cancer. Stem cells and development. 2012; 21:2355–2363. [PubMed: 22530882]

14. Shi Y, Hu G, Su J, et al. Mesenchymal stem cells: a new strategy for immunosuppression and tissue repair. Cell Res. 2010; 20:510–518. [PubMed: 20368733]

15. Amado LC, Saliaris AP, Schuleri KH, et al. Cardiac repair with intramyocardial injection of allogeneic mesenchymal stem cells after myocardial infarction. Proceedings of the National Academy of Sciences of the United States of America. 2005; 102:11474–11479. [PubMed: 16061805]

16. Ramdasi S, Sarang S, Viswanathan C. Potential of Mesenchymal Stem Cell based application in Cancer. International Journal of Hematology-Oncology and Stem Cell Research. 2015; 9:95–103. [PubMed: 25922650]

17. Studeny M, Marini FC, Champlin RE, Zompetta C, Fidler IJ, Andreeff M. Bone marrow-derived mesenchymal stem cells as vehicles for interferon-beta delivery into tumors. Cancer research. 2002; 62:3603–3608. [PubMed: 12097260]

18. Klopp AH, Lacerda L, Gupta A, et al. Mesenchymal Stem Cells Promote Mammosphere Formation and Decrease E-Cadherin in Normal and Malignant Breast Cells. PLoS ONE. 2010; 5:e12180. [PubMed: 20808935]

19. Park JS, Yang HN, Woo DG, Jeon SY, Park KH. Chondrogenesis of human mesenchymal stem cells in fibrin constructs evaluated in vitro and in nude mouse and rabbit defects models. Biomaterials. 2011; 32:1495–1507. [PubMed: 21122912]

20. Lee JM, Kim BS, Lee H, Im GI. In Vivo Tracking of Mesechymal Stem Cells Using Fluorescent Nanoparticles in an Osteochondral Repair Model. Mol Ther. 2012; 20:1434–1442. [PubMed: 22491215]

21. Azene N, Fu Y, Maurer J, Kraitchman DL. Tracking of stem cells in vivo for cardiovascular applications. Journal of Cardiovascular Magnetic Resonance. 2014; 16:1–22. [PubMed: 24387349]

22. Yuan H, Fales AM, Vo-Dinh T. TAT peptide-functionalized gold nanostars: enhanced intracellular delivery and efficient NIR photothermal therapy using ultralow irradiance. Journal of the American Chemical Society. 2012; 134:11358–11361. [PubMed: 22734608]

23. Yuan H, Khoury CG, Hwang H, Wilson CM, Grant GA, Vo-Dinh T. Gold nanostars: surfactant-free synthesis, 3D modelling, and two-photon photoluminescence imaging. Nanotechnology. 2012; 23:075102. [PubMed: 22260928]
24. Kong B, Seog JH, Graham LM, Lee SB. Experimental considerations on the cytotoxicity of nanoparticles. Nanomedicine (London, England). 2011; 6:929–941.
25. Yuan H, Gomez JA, Chien JS, et al. Tracking mesenchymal stromal cells using an ultra-bright TAT-functionalized plasmonic-active nanoplatform. Journal of Biophotonics. 2015:n/a–n/a.
26. Liu B, Li C, Cheng Z, Hou Z, Huang S, Lin J. Functional nanomaterials for near-infrared-triggered cancer therapy. Biomaterials science. 2016
27. Liu Y, Yang M, Zhang J, et al. Human Induced Pluripotent Stem Cells for Tumor Targeted Delivery of Gold Nanorods and Enhanced Photothermal Therapy. ACS nano. 2016; 10:2375–2385. [PubMed: 26761620]
28. Stuckey DW, Shah K. Stem cell-based therapies for cancer treatment: separating hope from hype. Nature reviews Cancer. 2014; 14:683–691. [PubMed: 25176333]
29. McCloy RA, Rogers S, Caldon CE, Lorca T, Castro A, Burgess A. Partial inhibition of Cdk1 in G 2 phase overrides the SAC and decouples mitotic events. Cell cycle (Georgetown, Tex). 2014; 13:1400–1412.
30. Schneider CA, Rasband WS, Eliceiri KW. NIH Image to ImageJ: 25 years of image analysis. Nature methods. 2012; 9:671–675. [PubMed: 22930834]
31. Murphy CJ, Gole AM, Stone JW, et al. Gold Nanoparticles in Biology: Beyond Toxicity to Cellular Imaging. Accounts of Chemical Research. 2008; 41:1721–1730. [PubMed: 18712884]
32. Jain S, Hirst DG, O'Sullivan JM. Gold nanoparticles as novel agents for cancer therapy. The British journal of radiology. 2012; 85:101–113. [PubMed: 22010024]
33. Vo-Dinh T, Fales A, Griffin GD, et al. Plasmonic Nanoprobes: From Chemical Sensing to Medical Diagnostics and Therapy. Nanoscale. 2013; 5:10127–10140. [PubMed: 24056945]
34. Wust P, Hildebrandt B, Sreenivasa G, et al. Hyperthermia in combined treatment of cancer. The Lancet Oncology. 2002; 3:487–497. [PubMed: 12147435]
35. Kennedy LC, Bickford LR, Lewinski NA, et al. A new era for cancer treatment: Gold-nanoparticle-mediated thermal therapies. Small. 2011; 7:169–183. [PubMed: 21213377]
36. Shakshouk HA, Rashwan H. Can mesenchymal stem cells be used as a future weapon against breast cancer? Alexandria Journal of Medicine.
37. Krishnamurthy S, Ke X, Yang YY. Delivery of therapeutics using nanocarriers for targeting cancer cells and cancer stem cells. Nanomedicine. 2015; 10:143–160. [PubMed: 25597774]
38. Lee DH, Ahn Y, Kim SU, et al. Targeting rat brainstem glioma using human neural stem cells and human mesenchymal stem cells. Clinical cancer research : an official journal of the American Association for Cancer Research. 2009; 15:4925–4934. [PubMed: 19638465]
39. Jang YY, Ye Z, Cheng L. Molecular imaging and stem cell research. Molecular imaging. 2011; 10:111–122. [PubMed: 21439256]
40. Fu Y, Azene N, Xu Y, Kraitchman DL. Tracking stem cells for cardiovascular applications in vivo: focus on imaging techniques. Imaging in medicine. 2011; 3:473–486. [PubMed: 22287982]
41. Frangioni JV, Hajjar RJ. In vivo tracking of stem cells for clinical trials in cardiovascular disease. Circulation. 2004; 110:3378–3383. [PubMed: 15557385]
42. Jang B, Park JY, Tung CH, Kim IH, Choi Y. Gold nanorod-photosensitizer complex for near-infrared fluorescence imaging and photodynamic/photothermal therapy in vivo. ACS nano. 2011; 5:1086–1094. [PubMed: 21244012]
43. Liu Y, Chang Z, Yuan H, Fales AM, Vo-Dinh T. Quintuple-modality (SERS-MRI-CT-TPL-PTT) plasmonic nanoprobe for theranostics. Nanoscale. 2013; 5:12126–12131. [PubMed: 24162005]
44. Yuan H, Khoury CG, Wilson CM, Grant GA, Bennett AJ, Vo-Dinh T. In vivo particle tracking and photothermal ablation using plasmon-resonant gold nanostars. Nanomedicine: Nanotechnology, Biology and Medicine. 2012; 8:1355–1363.
45. Higuchi T, Anton M, Dumler K, et al. Combined reporter gene PET and iron oxide MRI for monitoring survival and localization of transplanted cells in the rat heart. Journal of nuclear medicine : official publication, Society of Nuclear Medicine. 2009; 50:1088–1094.

46. Zhang SJ, Wu JC. Comparison of imaging techniques for tracking cardiac stem cell therapy. Journal of nuclear medicine : official publication, Society of Nuclear Medicine. 2007; 48:1916–1919.
47. Gao N, Chen Y, Li L, et al. Shape-Dependent Two-Photon Photoluminescence of Single Gold Nanoparticles. The Journal of Physical Chemistry C. 2014; 118:13904–13911.
48. Resch-Genger U, Grabolle M, Cavaliere-Jaricot S, Nitschke R, Nann T. Quantum dots versus organic dyes as fluorescent labels. Nat Meth. 2008; 5:763–775.
49. Huang K, Ma H, Liu J, et al. Size-Dependent Localization and Penetration of Ultrasmall Gold Nanoparticles in Cancer Cells, Multicellular Spheroids, and Tumors in Vivo. ACS nano. 2012; 6:4483–4493. [PubMed: 22540892]
50. Oh E, Delehanty JB, Sapsford KE, et al. Cellular Uptake and Fate of PEGylated Gold Nanoparticles Is Dependent on Both Cell-Penetration Peptides and Particle Size. ACS nano. 2011; 5:6434–6448. [PubMed: 21774456]
51. Niu W, Chua YAA, Zhang W, Huang H, Lu X. Highly Symmetric Gold Nanostars: Crystallographic Control and Surface-Enhanced Raman Scattering Property. Journal of the American Chemical Society. 2015; 137:10460–10463. [PubMed: 26259023]
52. Kolja T, Salamon J, Szwargulski P, et al. Increasing the sensitivity for stem cell monitoring in system-function based magnetic particle imaging. Physics in Medicine and Biology. 2016; 61:3279. [PubMed: 27032447]
53. Ariza de Schellenberger A, Kratz H, Farr TD, et al. Labeling of mesenchymal stem cells for MRI with single-cell sensitivity. International journal of nanomedicine. 2016; 11:1517–1535. [PubMed: 27110112]
54. Liu S, Tay LM, Anggara R, Chuah YJ, Kang Y. Long-Term Tracking Mesenchymal Stem Cell Differentiation with Photostable Fluorescent Nanoparticles. ACS Applied Materials & Interfaces. 2016
55. Madsen SJ, Baek SK, Makkouk AR, Krasieva T, Hirschberg H. Macrophages as cell-based delivery systems for nanoshells in photothermal therapy. Annals of biomedical engineering. 2012; 40:507–515. [PubMed: 21979168]
56. Schnarr K, Mooney R, Weng Y, et al. Gold nanoparticle-loaded neural stem cells for photothermal ablation of cancer. Advanced healthcare materials. 2013; 2:976–982. [PubMed: 23592703]
57. Durymanov MO, Rosenkranz AA, Sobolev AS. Current Approaches for Improving Intratumoral Accumulation and Distribution of Nanomedicines. Theranostics. 2015; 5:1007–1020. [PubMed: 26155316]
58. England CG, Gobin AM, Frieboes HB. Evaluation of uptake and distribution of gold nanoparticles in solid tumors. The European Physical Journal Plus. 2015; 130:1–16.
59. Nakamizo A, Marini F, Amano T, et al. Human bone marrow-derived mesenchymal stem cells in the treatment of gliomas. Cancer research. 2005; 65:3307–3318. [PubMed: 15833864]
60. Auffinger B, Morshed R, Tobias A, Cheng Y, Ahmed AU, Lesniak MS. Drug-Loaded Nanoparticle Systems And Adult Stem Cells: A Potential Marriage For The Treatment Of Malignant Glioma? Oncotarget. 2013; 4:378–396. [PubMed: 23594406]
61. Tsuji W, Rubin JP, Marra KG. Adipose-derived stem cells: Implications in tissue regeneration. World Journal of Stem Cells. 2014; 6:312–321. [PubMed: 25126381]
62. Wang X, Li G, Ding Y, Sun S. Understanding the photothermal effect of gold nanostars and nanorods for biomedical applications. RSC Advances. 2014; 4:30375–30383.

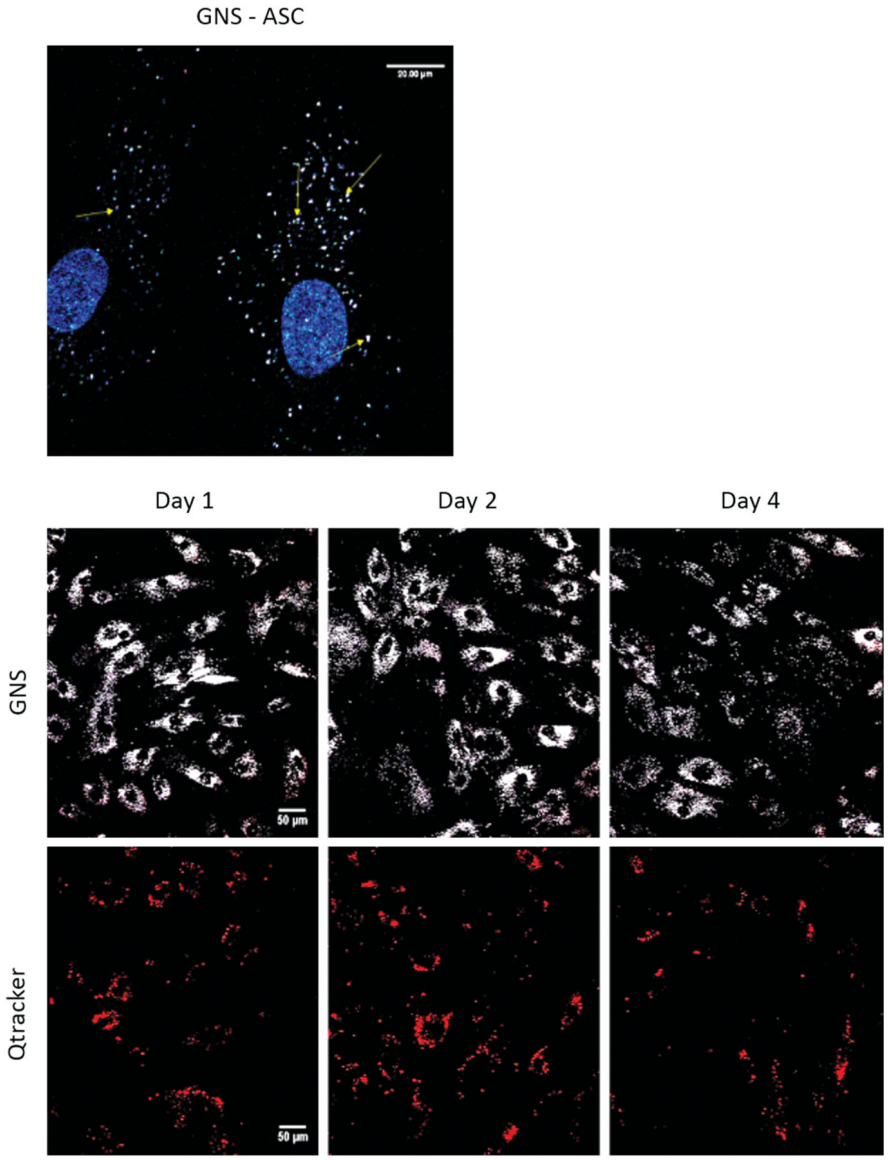

Figure 1.

Comparison of TPL in GNS vs. Qtracker labeled ASCs. Undifferentiated ASCs are shown stained with Hoechst33342 following a 24 hour incubation with 0.14nM GNSs, and imaged with MPM (*top*, scale bars = 20 μm). The cytoplasmic localization of the GNSs (yellow arrows), in relation to the nucleus that is stained blue is shown following imaging with MPM. Undifferentiated ASCs are shown following a 24 hour incubation with 0.14nM GNSs and 0.14nM Qtracker (*bottom*, scale bars = 50μm). Cells were fixed on days 1, 2, and 4 and then imaged to determine the relative fluorescence of each optical label. Each cell could be roughly distinguished by its predominant fluorescence. Qtracker (red) and GNSs (white) could be seen in each cell. Fluorescence was measured over a period of 4 days. Calculated total cell fluorescence (CTCF) was calculated with ImageJ and analyzed using a two-way ANOVA. There was a significantly greater degree of fluorescence emitted by those cells

labeled with GNSs vs. Qtracker throughout all 4 days of cellular proliferation. ($P<0.0001$). MPM images were taken at 800nM using a laser power of 3.7mW.

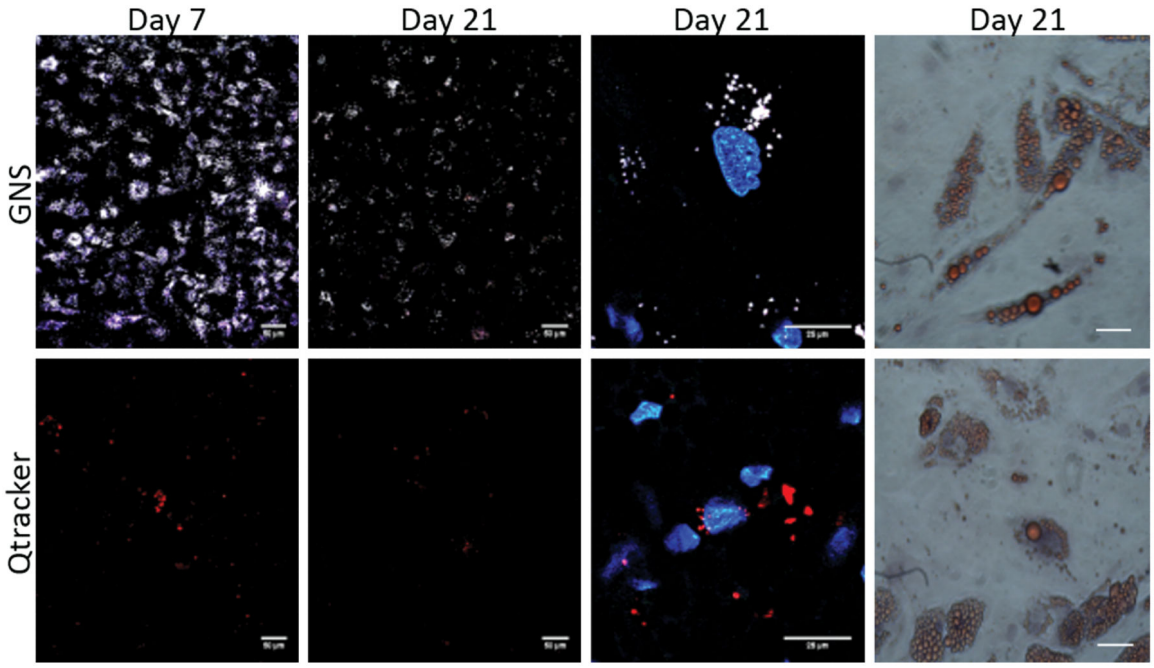

Figure 2.

ASC adipogenic differentiation following labeling with GNSs and Qtracker. For all studies, ASCs were incubated with 0.14nM GNSs and 0.14nM Qtracker for 24 hours prior to differentiation. In columns 1 and 2, for adipogenesis on the 7th and 21st day of differentiation, images were taken with MPM to monitor the TPL of the labels (scale bars = 50μm). Images in the third column show labeled ASCs on the 21st day of differentiation at 5× zoom with GNSs and Qtracker (scale bars = 25μm). Images in the third column were stained with Hoechst33342. The last column represents the confirmation of phenotypic differentiation with Oil Red O for adipogenesis (scale bars = 100μm). For adipogenesis, the cells labeled with GNSs could be easily visualized over a period of 21 days and to a greater extent than with the Qtracker label. Results similar to those shown in this figure were seen in osteogenesis and chondrogenesis as well. All samples were imaged with MPM using a wavelength of 800nM at 3.7mW.

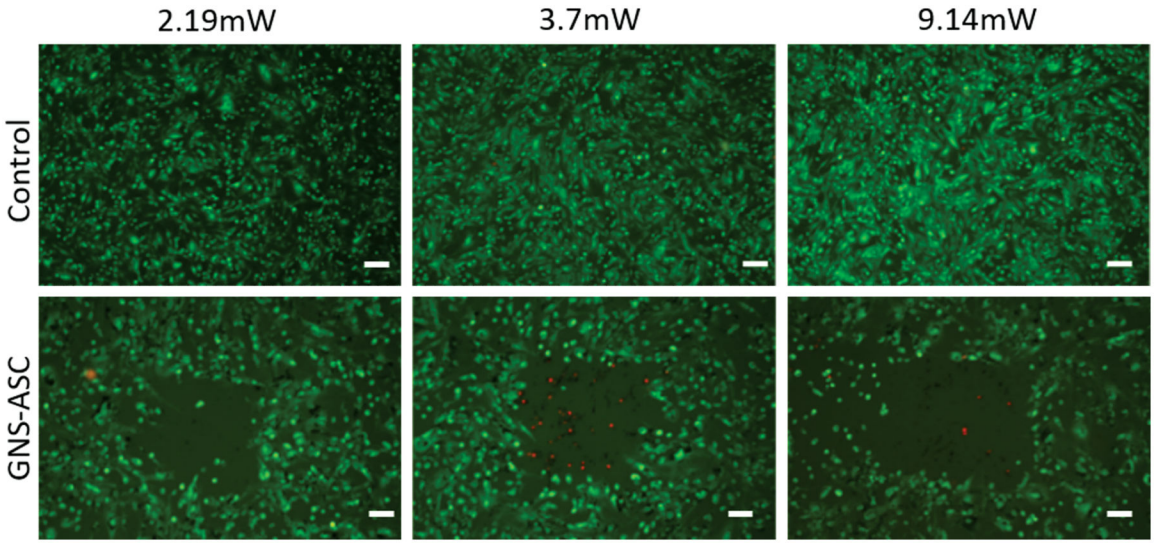

Figure 3.

Photothermal therapy effects on GNS-ASCs in monoculture. ASCs were incubated with unlabeled medium (control) and GNSs for 24 hours at 37 °C, and then exposed to an 800nm laser for 3 minutes using MPM. The laser powers used were 2.19mW, 3.7mW, and 9.14mW. Cells were stained with fluorescein diacetate and propidium iodide which stain live cells green and dead cells red respectively; representative images are shown following laser exposure (scale bars = 100μm). The control group displayed no cell death at all treatment powers. The empty area in the center of the images of GNS-ASCs demonstrates a clear zone of cellular ablation. A treatment power of 3.7mW was found to be the most efficient and specific with respect to the size and area of ablation. This power was selected for use in the co-culture photothermal treatments.

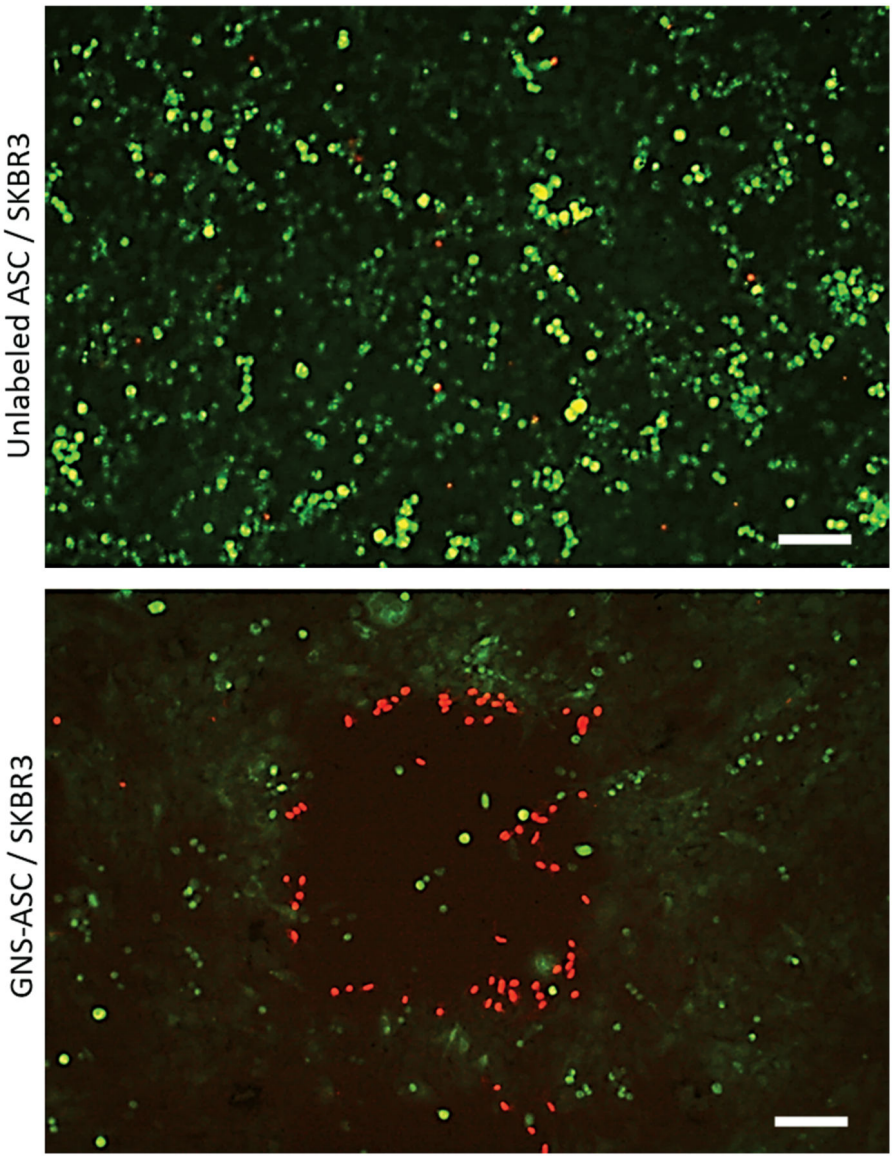

Figure 4.

Photothermal therapy effects on GNS-ASCs and SKBR3 breast cancer cell co-cultures (scale bars = 100μm). SKBR3 cells were co-cultured with either GNS-ASCs, or ASCs alone (control) for 24 hours and then exposed to a 3.7mW laser for 3 minutes using the MPM. As compared to the unlabeled ASCs, those cells co-cultured with GNS-ASCs demonstrated a clear area of cellular death following treatment. Both samples were stained with fluorescein diacetate and propidium iodide. All images are 1.86×1.24 mm^2.